Human Molecular Genetics, 2016, Vol. 25, No. 16 3416–3431

doi: 10.1093/hmg/ddw184
Advance Access Publication Date: 21 June 2016
Original Article

ORIGINAL ARTICLE

Functional rescue of REP1 following treatment with PTC124 and novel derivative PTC-414 in human choroideremia fibroblasts and the nonsense-mediated zebrafish model

Mariya Moosajee[1,2,3,*], Dhani Tracey-White[1], Matthew Smart[1], Marla Weetall[4], Simona Torriano[5], Vasiliki Kalatzis[5], Lyndon da Cruz[1,2], Peter Coffey[1], Andrew R. Webster[1,2] and Ellen Welch[4]

[1]UCL Institute of Ophthalmology, London EC1V 9EL, UK, [2]Moorfields Eye Hospital NHS Foundation Trust, London EC1V 2PD, UK, [3]Great Ormond Street Hospital, London WC1N 3JH, UK, [4]PTC Therapeutic Inc, NJ, USA and [5]Inserm U1051, Institute for Neurosciences of Montpellier, Montpellier cedex 5, France

*To whom correspondence should be addressed at: UCL Institute of Ophthalmology, 11-43 Bath Street, London EC1V 9EL, UK. Tel: +44 (0) 207 608 6971; Fax: +44 (0) 207 608 6830; Email: m.moosajee@ucl.ac.uk

Abstract

Choroideremia (CHM) is an X-linked chorioretinal dystrophy that is caused by mutations within a single gene, *CHM*. Currently no effective treatment exists for these patients. Since over 30% of patients harbour nonsense mutations in *CHM*, nonsense suppression therapy using translational readthrough inducing drugs may provide functional rescue of REP1, thus attenuating progressive sight loss. Here, we employed two CHM model systems to systematically test the efficacy and safety of ataluren (PTC124) and its novel analog PTC-414: (1) the *chm*^{ru848} zebrafish, the only nonsense mutation animal model of CHM harbouring a TAA nonsense mutation, and (2) a primary human fibroblast cell line from a CHM patient harbouring a TAG nonsense mutation. PTC124 or PTC-414 treatment of *chm*^{ru848} embryos led to a ~2.0-fold increase in survival, prevented the onset of retinal degeneration with reduced oxidative stress and apoptosis, increased rep1 protein by 23.1% (PTC124) and 17.2% (PTC-414) and restored biochemical function as confirmed through *in vitro* prenylation assays (98 ± 2% [PTC124] and 68 ± 5% [PTC-414]). In *CHM*$^{Y42X/y}$ fibroblasts, there was a recovery of prenylation activity following treatment with either PTC124 (42 ± 5%) or PTC-414 (36 ± 11%), although an increase in REP1 protein was not detected in these cells, in contrast to the zebrafish model. This comprehensive study on the use of PTC124 and PTC-414 as successful nonsense suppression agents for the treatment of CHM highlights the translational potential of these drugs for inherited retinal disease.

Introduction

Choroideremia (CHM) is an X-linked recessive inherited chorioretinal dystrophy caused by mutations in the *CHM* gene, that spans a genomic sequence of ~150 kb on chromosome Xq21.2, containing 15 exons and encoding a ubiquitously expressed protein of 653 amino acids; Rab Escort Protein 1 (REP1). REP1 is an essential component of the catalytic Rab geranyl-geranyl transferase (RGGTase) II complex, and is involved in lipid modification

Received: February 20, 2016. **Revised:** June 3, 2016. **Accepted:** June 6, 2016

(prenylation) of Rab proteins and facilitates their intracellular membrane transport trafficking by binding to the hydrophobic prenylation motifs at the C termini [1] There are over 50 Rab proteins, present in all cells. Within the retina, they act to transport melanosomes within the retinal pigment epithelium (RPE) and assist phagocytosis of disc membranes shed from the outer segments. There have been over 200 unique mutations involving *CHM* reported in the Human Gene Mutation Database and characterization of the mutation spectrum reveals 30% are nonsense mutations resulting in premature termination codons (PTCs) [2]. Humans have two REP isoforms, REP1 and REP2 (encoded by the retrogene choroideremia-like, *CHML*, located on chromosome 1), which share 75% amino acid identity, enabling Rabs to competitively bind to one or the other. However, a subset of Rabs have been found to be prenylated less efficiently by REP2 than by REP1 i.e. Rab27a exhibits a 4-fold difference and Rab7 shows a >6-fold difference [3]. This has led to the proposal that loss of function *CHM* mutations reduce the amount of total REP activity, shifting prenylation towards REP2. In the retina, where there is active synthesis of multiple Rabs, competitive binding results in underprenylation of low affinity Rabs, such as Rab27a, resulting in a subsequent retinal degeneration.

Affected male patients typically develop early onset night blindness in childhood, followed by restriction of the peripheral visual field, and finally a decrease in central visual acuity, often leading to complete blindness during the fifth to sixth decade of life [4]. Female carriers may be asymptomatic, or display patchy areas of chorioretinal atrophy that represent clonal areas of the disease due to random X-inactivation. However, later in life, carrier females can often develop night blindness and field loss because of expanding areas of chorioretinal atrophy.

In order to test the safety, efficacy and application of small molecule translational readthrough inducing drugs (TRIDs) for the potential treatment of inherited retinal disease, CHM was selected as a prototype given its causative preponderance of nonsense mutations. In this study, we used two independent disease models of CHM. First, a human primary fibroblast cell line, derived from a CHM patient with a nonsense mutation resulting in absent REP1 and loss of prenylation function, therefore acting as a suitable cellular model for testing pharmacological therapies. Second, in order to study the effect of drug treatment on the entire retina, the *in vivo* chm^{ru848} zebrafish was used. This is the only animal model of CHM with a nonsense mutation in the *chm* gene, resulting in a UAA stop codon, p.Q32X in exon 2. [5] Zebrafish possess only one rep isoform, which shares 55% homology with human REP1. The lack of a second rep isoform to compensate in tissues other than the eye, analogous to human REP2, leads to a multisystemic disease in zebrafish resulting in embryonic lethality by a mean 4.8 ± 1.0 days post-fertilization (dpf). The retinal degeneration is well-characterized with the first signs emerging as patchy areas of RPE hypertrophy and atrophy at 4.5 dpf followed by a widespread severe degeneration with loss of retinal lamination and high levels of cell death by 5 dpf. This is due to the loss of maternal *rep1* mRNA and protein present in the yolk sac that supports normal development up till 4 dpf [5]. Any therapy that can increase rep1 protein will have a global effect on the fish without any confounding factors. This model has been successfully used previously to highlight the efficient readthrough of traditional aminoglycosides, paromomycin and gentamicin [6]. Using this model also allows other systemic drug side effects including oto- and renal toxicity to be investigated.

Ataluren (PTC124) was discovered through high-throughput screens utilizing premature UGA luciferase (LUC) reporters in either stably transfected HEK293 cells or rabbit reticulocyte lysates. Chemical optimization of hit molecules using nonsense-containing cell and animal models and preclinical safety assessments ultimately resulted in the selection of PTC124 as a clinical candidate. Further chemical optimization to increase plasma exposure and tissue penetration was performed using a similar screening tier as PTC124. Compounds that manifested increased readthrough activity at UGA, UAA and UAG codons with minimal cellular toxicity were characterized further for their relative potency, activity and pharmaceutical properties. These studies led to the identification of several lead compound classes that were further chemically optimized. PTC-414 was identified as a compound that maintained the favourable properties of PTC124, but improved the potency, pharmacokinetic properties and the readthrough at all three stop codons (Table 1).

In this study, we test these two small molecule TRIDs, PTC124 and PTC-414, to compare their level of translational readthrough in two independent *in vitro* and *in vivo* disease models of choroideremia.

Table 1. Characteristics of PTC124 and PTC-414

Activity	Compound	
	PTC124	**PTC-414**
UGA readthrough (fold over DMSO[a]) in LUC reporter assay[b]	4.1 fold	6.3 fold
UAA readthrough (fold over DMSO[a]) in LUC reporter assay[b]	1.1 fold	2.4 fold
UAG readthrough (fold over DMSO[a]) in LUC reporter assay[b]	1.0 fold	2.0 fold
Activity in human liver microsome assay to assess *in vitro* drug metabolism (% lost after 1 h incubation)	<10% metabolized	12% metabolized
Mouse plasma exposure (10 mg/kg oral dose)[c]		
1 h after 10 mg/kg oral dose of compound	0.87 μg/ml	0.41 μg/ml
3 h after 10 mg/kg oral dose of compound	0.17 μg/ml	0.22 μg/ml
6 h after 10 mg/kg oral dose of compound	0.04 μg/ml	0.19 μg/ml
CC_{50} in LLC-PK1 (kidney proximal tubule) cells[d]	>100 μM	>100 μM

[a]DMSO: dimethyl sulfoxide used as solvent.

[b]LUC reporter containing indicated stop codon at amino acid position 190 as described previously in [10].

[c]Plasma concentration at each time interval after a 10 mg/kg dose of compound was quantified by LC-MS/MS.

[d]CC_{50}, cytotoxic effects of compounds in LLC-PK1 cells were expressed as the 50% cytostatic concentration (CC_{50}), defined as the concentration required to reduce cell growth by 50%.

Results

Therapeutic dose of TRIDs for the chm^{ru848} zebrafish model

To determine the highest dose of drug that could be safely tolerated in zebrafish, we carried out survival experiments.

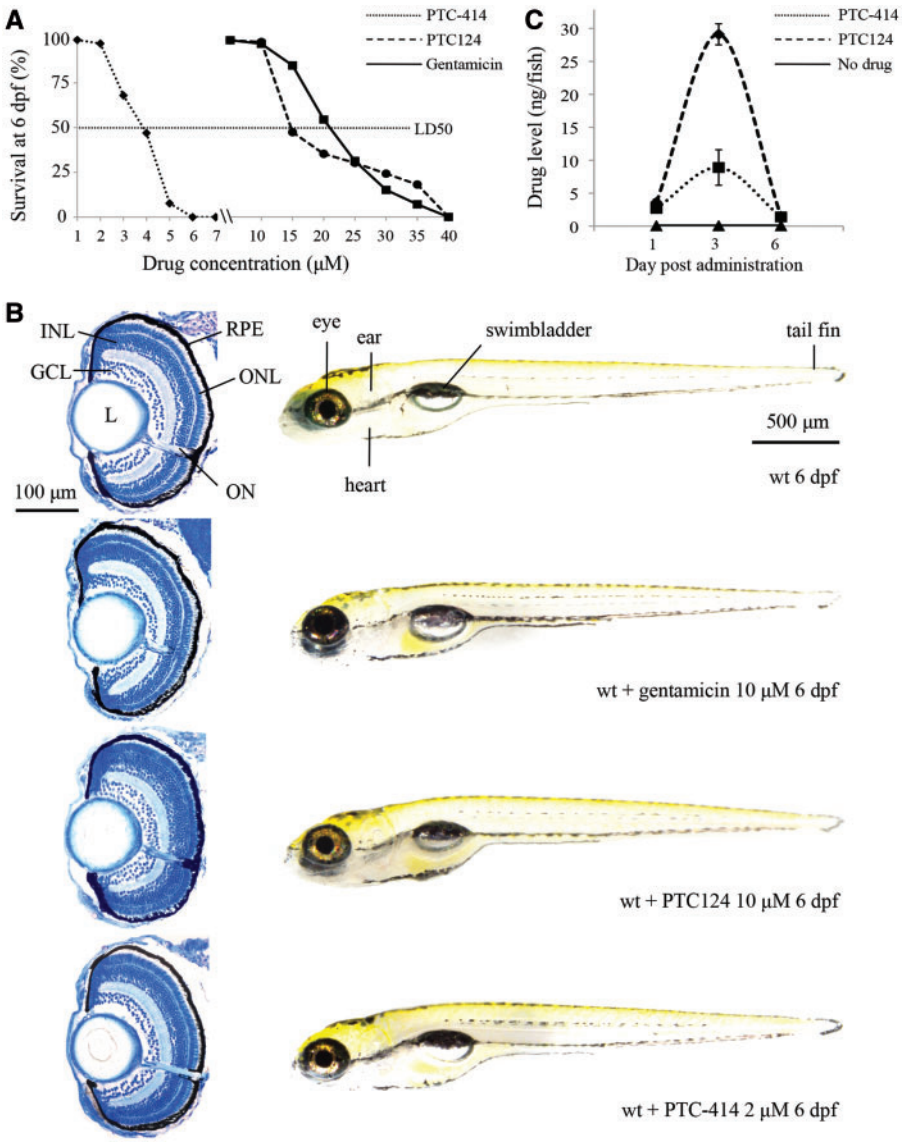

Figure 1. Dose–response studies. **(A)** wt embryos dosed at 10 hpf with gentamicin (solid line), PTC124 (dashed line) or PTC-414 (dotted line). Percentage survival at 6 dpf was determined for each treatment group, $n = 3$ (30 embryos/group), mean ± SEM. Error bars smaller than the symbol are not visible. **(B)** Coronal retinal sections and wholemount morphology of wt larvae at 6 dpf with or without treatment with 10 μM gentamicin, 10 μM PTC124 or 2 μM PTC-414. RPE, retinal pigment epithelium; INL, inner nuclear layer; L, lens; GCL, ganglion cell layer; ONL, outer nuclear layer; ON, optic nerve. **(C)** Levels of drug in wt fish after a single dose at 10 hpf with 10 μM PTC124 (dashed line) or 2 μM PTC-414 (dotted line) compared with undosed fish (solid black line) at day 1, 3 and 6 post-administration.

The survival of wildtype (wt) embryos dosed continuously from 10 hours post-fertilization (hpf), prior to eye development, with PTC124 and PTC-414 (0.025–50 μM) was measured at 6 dpf (Fig. 1A). Median lethal dose (LD50) was 15 μM for PTC124 and 4 μM for PTC-414. The potency of the gentamicin solution differed from previous experiments hence the dose response curve was repeated to determine the optimum dose, and was found to be 10 μM with a LD50 of 21 μM (Fig. 1A). Embryos treated with 10 μM gentamicin, 10 μM PTC124 and 2 μM PTC-414 displayed 98.7 ± 1.3% survival rates (in line with natural survival rates of untreated wt embryos) at 6 dpf with normal gross morphology and retinal histology (Fig. 1B). There was no difference in gross behaviour between untreated and treated wt embryos, all demonstrating normal stereotyped motor behaviours that allow them to navigate their environment including slow and fast swimming bouts, with no signs of imbalance or lack of movement. Following single dose administration of 10 μM PTC124 and 2 μM PTC-414 to wt embryos at 10 hpf (20 embryos per group, with three biological replicates), the concentration of PTC124 and PTC-414 was measured at day 1, 3 and 6 (Fig. 1C). Both drugs reached a peak at day 3 with PTC124 reaching a mean of 29 ng/fish (0.1 nmole/fish) and PTC-414 8.9 ng/fish (0.02 nmole/fish), both tapered off by day 6 although the drugs were still detectable compared with undosed fish.

Renal- and oto-toxic assays for TRIDs

Although PTC derivatives are unrelated to aminoglycosides, which cause significant renal and ototoxicity, these parameters were tested to complement the morphological, behavioural and

retinal safety profile. Pronephric tubule filtration efficiency, as a measure of renal function, was tested by injecting rhodamine-labelled 10 kDa dextran into the pericardial sac of untreated and treated wt fish and measuring the transit of dye out of the circulation, which if normal occurs through the glomerulus with excretion in the urine (Fig. 2A and B). PTC124 (10 μM) showed no signs of toxicity with good filtration efficiency (37.6 ± 1.7%) comparable to wt levels (38.6 ± 3.2%). PTC-414 (2 μM) demonstrated a degree of renal dysfunction (68.8 ± 3.1%), which was significantly higher than PTC124 and wt fish ($P < 0.01$), but not as severe as gentamicin (10 μM), where 94.7 ± 5.5% of the dye failed to be excreted by the embryos.

The lateral line neuromast mechanosensory hair cells of larval zebrafish were used as an *in vivo* surrogate model of mammalian inner ear hair cells to test ototoxicity of PTC124 and PTC-414. Live embryos at 6 dpf were incubated with 4-Di-2-Asp, a fluorescent dye that is preferentially taken up by hair cells. Gentamicin is a known ototoxin and showed reduced staining and a statistically significant reduction in neuromast survival score of 0.5 ± 0.5, indicative of hair cell damage or loss (Fig. 2C and D). PTC124 (score 28.8 ± 3.8) and PTC-414 (score 30.4 ± 6.7) showed no significant reduction in the gross number of neuromasts relative to untreated larva.

In order to view the structural integrity and number of hair cells in the neuromasts, immunostaining with anti-acetylated tubulin, which labels the kinocilia, and phalloidin labelling of the stereocilia bundles was performed in fixed wt larva following drug exposure (Fig. 2D). We counted the hair cells in the opercular (OP) neuromast of 5 wt embryos from each treatment group, and found the mean number (± SD) of hair cells per neuromast at 6 dpf was 12.0 ± 3.5. This was in-line with previously published counts of 13.3 ± 2.94 [7]. This was markedly reduced for gentamicin-treated fish (1.2 ± 1.0, $P < 0.01$) compared with PTC124 (10.1 ± 3.6) and PTC-414-treated (9.4 ± 3.1) embryos.

TRID treatment increases the survival of *chm*^{ru848} mutants

On the basis of the results in wt fish, the effect of each compound on survival in *chm*^{ru848} mutants was determined following the administration of 10, 2 and 10 μM of PTC124, PTC-414 and gentamicin, respectively, at 10 hpf compared with untreated embryos (Fig. 3A). Untreated *chm*^{ru848} mutants survived an average of 4.8 ± 1.2 days, whereas *chm*^{ru848} embryos treated with PTC124 lived for 10.1 ± 1.6 days representing a 2.1-fold increase in survival. PTC-414 treated fish lived for 9.1 ± 1.7 days extending a 1.9-fold increase in survival, and gentamicin control fish lived for 8.2 ± 1.4 days with a 1.7-fold increase in survival. Treatment of *chm*^{ru848} mutant embryos with either drug significantly increased their survival time ($P < 0.01$) compared with untreated mutants; however, the difference between survival of gentamicin-treated and PTC derived-treatment groups was not significant. In order to confirm whether the 10 μM dose of PTC124 was optimum, *chm*^{ru848} embryos were dosed with 5 and 15 μM concentrations, the survival dropped to 5.6 ± 0.1 days and 5.3 ± 0.6 days, respectively, there was no significant difference from undosed mutants (Fig. 3B). In addition, dosing of *chm*^{ru848} embryos with 10 μM at 3 dpf did not improve their phenotype or their survival (6.0 ± 0.1 days). PTC-414 showed a narrow dose response with 32% lethality with 3 μM treatment at 10 hpf (Fig. 1A), and when dosed at 3 dpf with 2 μM there was also no improvement in survival (5.6 ± 0.4 days).

Effect of TRID treatment on *chm*^{ru848} morphology and retinal histology

Mutant *chm*^{ru848} larvae at 6 dpf displayed characteristic systemic defects such as pericardial and abdominal oedema, shorter body length (mean 2.81 ± 0.25 mm), an uninflated swim bladder, persistent yolk sac and microphthalmia (mean 228 ± 10 μm) with irregular darker eye pigmentation due to reduced iridophore pigment cells (Fig. 3C). Treatment with 10 μM PTC124 or 2 μM PTC-414 resulted in milder *chm*^{ru848} phenotypes at 6 dpf with reduced pericardial and abdominal oedema, significantly increased body length and larger eye diameter compared with untreated mutants ($P > 0.01$, Fig. 3C-E). There was no significant difference between treated *chm*^{ru848} and wt parameters (mean body length 3.85 ± 0.22 mm and mean eye diameter 310 ± 14 μm). Importantly, a functional inflated swim bladder failed to develop in treated mutants and this consequently impaired proper feeding, leading to starvation, as was seen in our previous study with aminoglycosides [6].

Coronal sections of the *chm*^{ru848} retina showed widespread degeneration with pyknotic cells (nuclear condensation appearing dark with overall loss of cytoplasm) throughout all layers of the retina, diminishing lamination, areas of RPE atrophy and hypertrophy and small cataractous lenses (Fig. 4A) [5]. Treated *chm*^{ru848} mutant retina at 6 dpf showed remarkable preservation of lamination including a regular RPE layer, absence of pyknotic cells and normal lens. The main difference between treated *chm*^{ru848} mutant and wt retina was notably thickened inner nuclear and ganglion cell layers (Fig. 4A). In addition, the ganglion cell layer was closely opposed to the lens in the treated mutants owing to ganglion cell proliferation. At 10 dpf, retinal sections appeared similar to wt fish, although the ganglion cell layer and inner nuclear layer remained increased with a higher density of nuclei, and reduction of the vitreous cavity (Fig. 4D). There were early signs of RPE hypertrophy in the PTC-414 treated retina, but no gross signs of photoreceptor degeneration.

Effect of TRID treatment on apoptotic cell death in zebrafish mutants

TUNEL assays were performed on coronal retinal sections of wt, untreated and treated *chm*^{ru848} embryos at 6 dpf to assess levels of cell death. In each mutant treated with either 10 μM PTC124 or 2 μM PTC-414 at 10 hpf ($n = 5$ per group), apoptotic activity was significantly reduced to wt levels within the retina ($P > 0.01$, Fig. 4A and B), which may have accounted for the thicker nuclear layers. The gentamicin treated retina did however display slightly higher levels of cell death predominantly in the RPE, photoreceptor layer and around the lens but still remained significantly lower compared with untreated mutants.

Oxidative stress in the *chm*^{ru848} eye

The superoxide-sensitive dye dihydroethidium (DHE) was used to semi-quantitatively evaluate the *in situ* generation of superoxide and thiobarbituric acid reactive substances as indicators of lipid peroxidation and oxidative stress in the eyes of wt and *chm*^{ru848} treated and untreated embryos (Fig. 4A and C). In untreated *chm*^{ru848} whole eyes, there were high levels of oxidative stress associated with the disease process itself (mean DHE fluorescence/eye 27.9 ± 1.1). Once dosed with PTC-derived small molecules, the reactive oxygen species (ROS) reduced significantly to wt levels ($P < 0.01$). Gentamicin is known to cause oxidative stress and the mean DHE fluorescence/eye was 12.1 ± 0.8

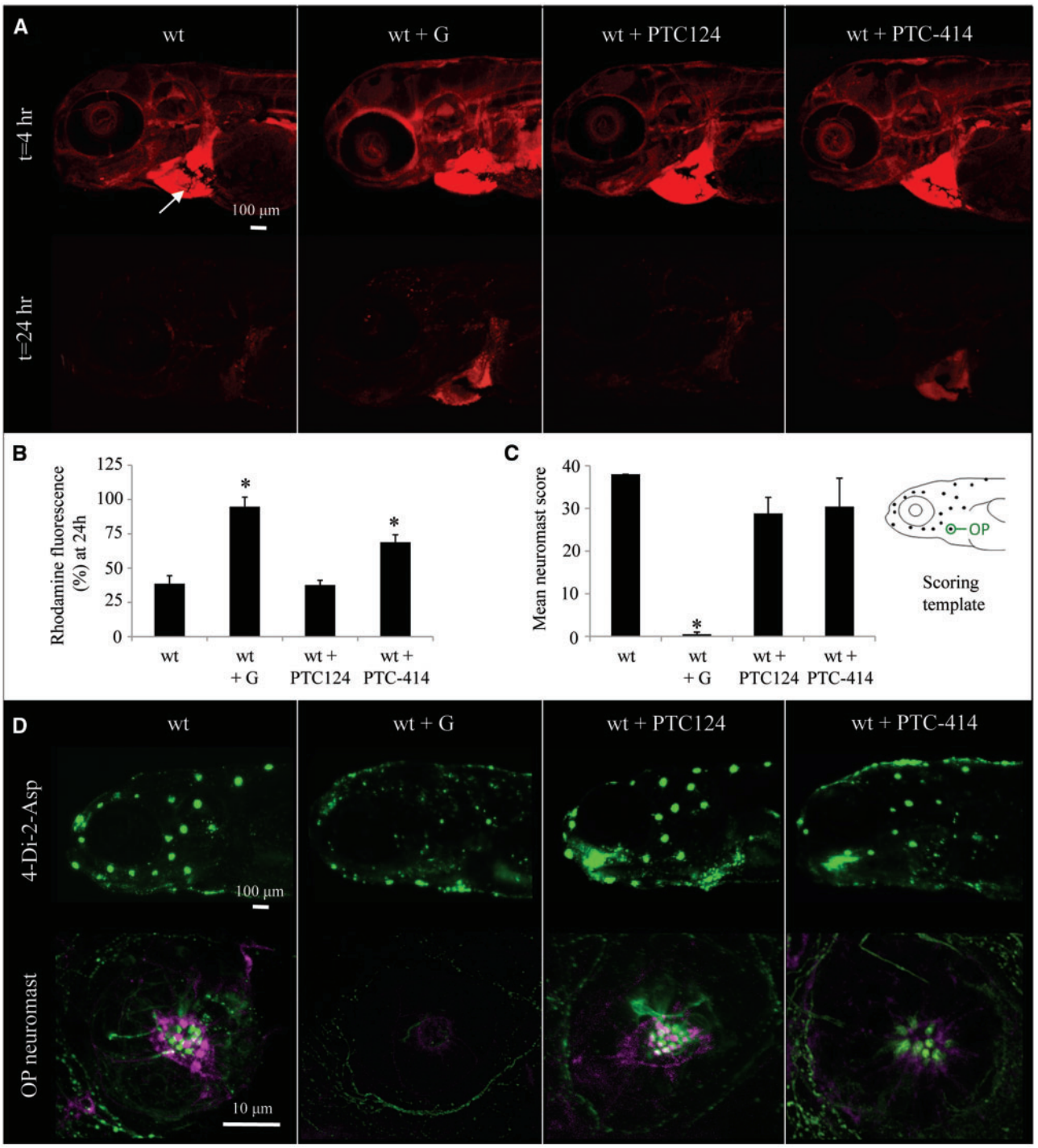

Figure 2. Renal- and oto-toxicity studies. **(A)** Fluorescent image of a wt embryo with or without treatment with 10 µM gentamicin (+G), 10 µM PTC124 (+ PTC124) or 2 µM PTC-414 (+ PTC-414), following injection of rhodamine dextran into the heart (white arrow) at 3 dpf. Top row is 4 h post-injection (t = 4 h) and bottom row is 24 h later (t = 24 h); **(B)** Graph quantifying the percentage of original rhodamine dextran fluorescence remaining in the circulation at 24 h after injection ($n = 5$ embryos for each group, mean ± SEM). **(C)** Neuromast survival from wt larvae at 6 dpf with or without treatment with 10 µM gentamicin (+G), 10 µM PTC124 (+ PTC124) or 2 µM PTC-414 (+ PTC-414) quantified with 4-Di-2-Asp scores, $n = 5$ embryos for each group, mean ± SD). The scoring template highlights the positions of the 19 head neuromasts. OP, opercular neuromast. 4-Di-2-Asp score for gentamicin treated fish was significantly decreased (*$P < 0.01$) compared with undosed and PTC-derivatives. **(D)** Lateral line neuromasts in the head region of wt larvae at 6 dpf with or without treatment with 10 µM gentamicin (+G), 10 µM PTC124 (+ PTC124) or 2 µM PTC-414 (+ PTC-414) stained with 4-Di-2-Asp (top row). The OP neuromast was imaged as a representative from each corresponding fixed 6 dpf wt larva (bottom row) containing double labelled hair cells with anti-acetylated tubulin (green, kinocilia) and phalloidin (purple, stereocilia bundles).

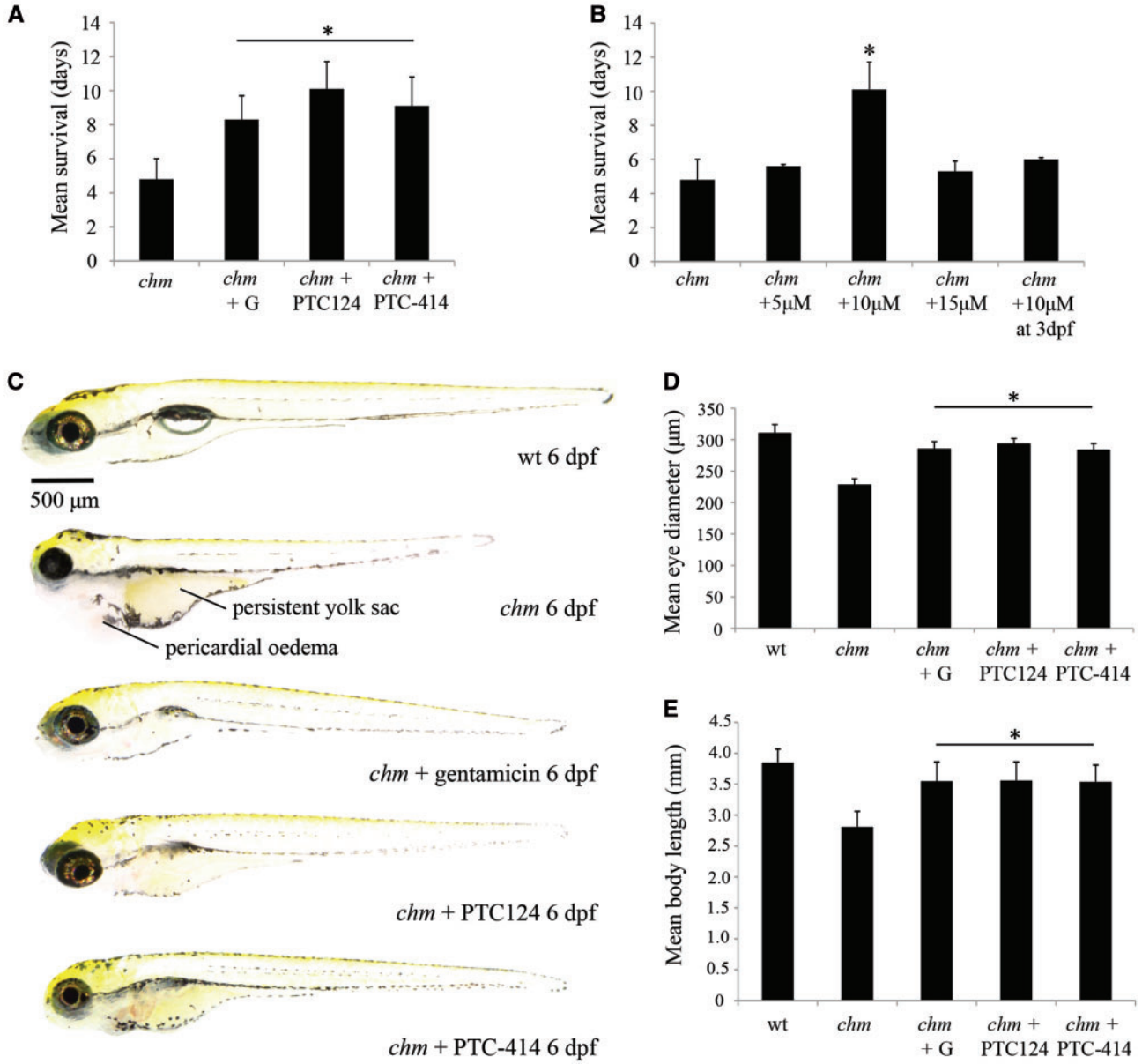

Figure 3. Survival studies. **(A)** Mean survival of *chm*^{ru848} mutant embryos (*chm*) with or without treatment with 10 μM gentamicin (+G), 10 μM PTC124 (+ PTC124) or 2 μM PTC-414 (+ PTC-414), $n = 50$ for each group, mean ± SEM. Statistical analysis of the data by pair-wise comparisons between the control untreated mutants and each treatment group was performed using the Mann–Whitney test, *$P < 0.01$. **(B)** Mean survival of *chm* embryos with or without treatment with 5, 10 and 15 μM PTC124 at 10 hpf, or 10 μM PTC124 at 3 dpf ($n = 30$ for each group, mean ± SEM). **(C)** Gross wholemount morphology of 6 dpf wt, *chm* untreated and treated with 10 μM gentamicin (+G), 10 μM PTC124 (+ PTC124) or 2 μM PTC-414 (+ PTC-414) embryos showing overall improvement in systemic appearance in treated fish. **(D)** Mean eye diameter (μm) and **(E)** mean body length (mm) of *chm* mutant embryos with or without treatment with 10 μM gentamicin (+G), 10 μM PTC124 (+ PTC124) or 2 μM PTC-414 (+ PTC-414) at 6 dpf ($n = 5$ for each group, mean ± SEM). Treated mutants showed a larger eye size and body length (*$P < 0.01$) compared with untreated *chm* embryos.

in wt embryos treated with 10 μM gentamicin [8]. But the generation of functional rep1 through its readthrough ability appears to have an overall treatment benefit, highlighted by the reduction of ROS in gentamicin treated mutants (mean DHE fluorescence/eye 17.4 ± 1.2) versus untreated *chm*^{ru848}, despite its toxic side effects.

Quantitative RT-PCR

Nonsense mediated decay (NMD) is a surveillance process that recognizes and selectively degrades PTC-containing mRNA. The level of NMD sensitivity is multifactorial resulting in a proportion of transcripts escaping the pathway. In order to detect the level of mRNA available for readthrough activity, quantitative RT-PCR was conducted using untreated *chm*^{ru848} embryos, revealing transcripts reached a mean 42 ± 6% of wt levels (Fig. 5A). When treated with PTC124, transcript levels rose to a mean 74 ± 9%; however, a similar increase was not observed following PTC-414 treatment with levels remaining at 49 ± 3%.

Patient *CHM*$^{Y42X/y}$ fibroblasts were derived from a skin biopsy of a 25-year-old male. The nonsense mutation c.126C > G (p.Y42X, UAG) was confirmed in the fibroblasts by direct sequencing. Untreated and treated *CHM*$^{Y42X/y}$ patient fibroblasts

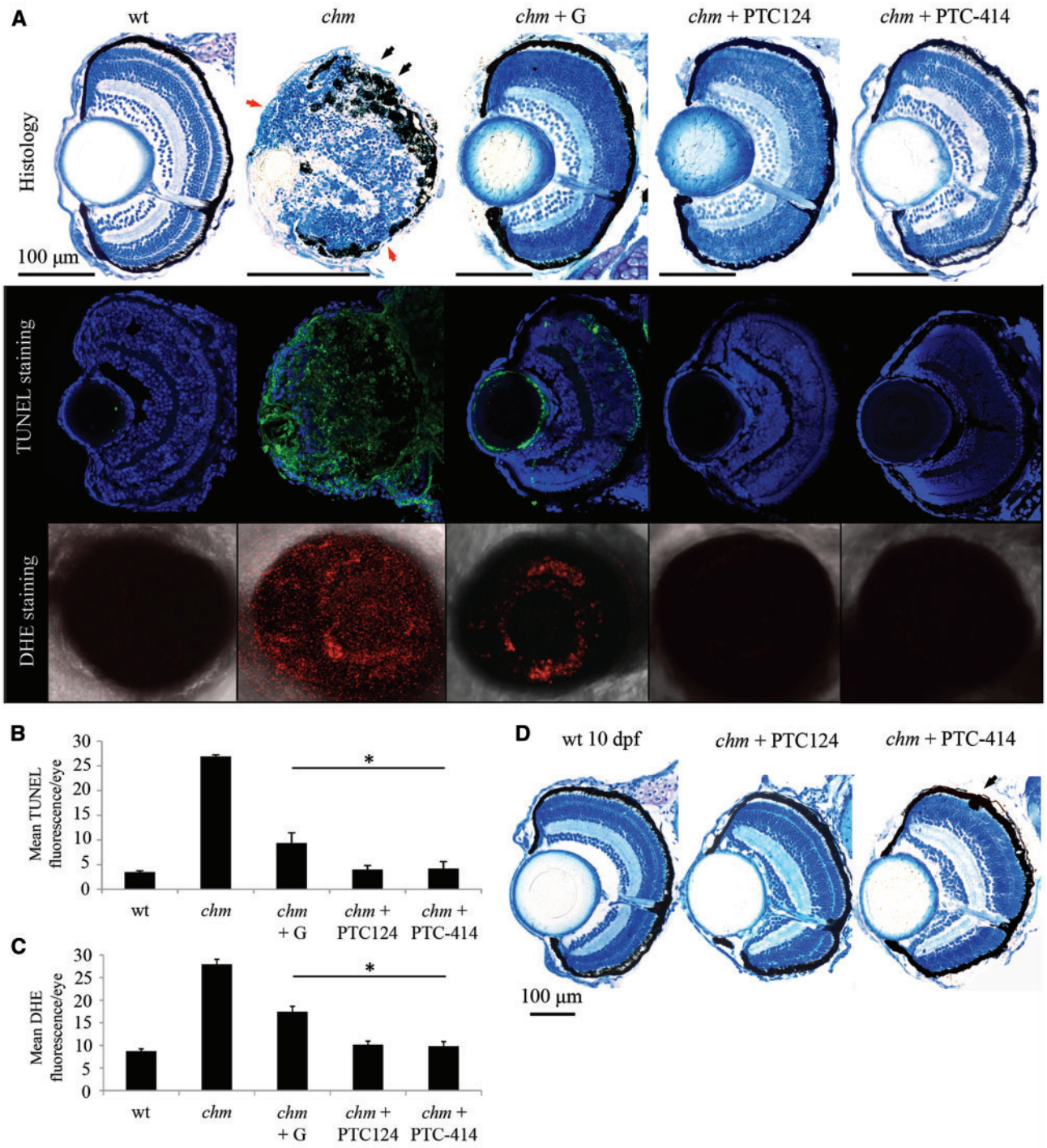

Figure 4. Retinal phenotyping of *chm*^{ru848} embryos treated with TRIDs. **(A)** Top row shows coronal retinal sections stained with 1% toluidine blue through wt and *chm* 6 dpf eyes with or without treatment with 10 μM gentamicin (+G), 10 μM PTC124 (+ PTC124) or 2 μM PTC-414 (+ PTC-414); middle row shows corresponding TUNEL staining at 6 dpf with undosed *chm* mutants displaying widespread TUNEL staining compared with wt and treated *chm* embryos; bottom row shows stacked confocal images of corresponding whole eyes with DHE staining highlighting levels of oxidative stress. **(B)** Mean TUNEL fluorescence/eye ± SEM derived from $n = 5$ embryos for each group, was analyzed using ImageJ. All treated *chm* mutants showed significantly less cell death than untreated *chm* embryos (*$P > 0.01$). **(C)** Mean DHE fluorescence/eye ± SEM derived from $n = 5$ embryos for each group, was analyzed using ImageJ. All three TRIDs reduce the level of oxidative stress in the eye compared with undosed *chm* mutants (*$P > 0.01$), but PTC-derived drugs were able to normalize to wt levels. **(D)** Coronal retinal sections through 10 dpf wt and *chm* eyes treated with 10 μM PTC124 (+ PTC124) or 2 μM PTC-414 (+ PTC-414). Red arrowheads point to areas of RPE atrophy and black arrowheads point to RPE hypertrophy. All scale bars represent 100 μm.

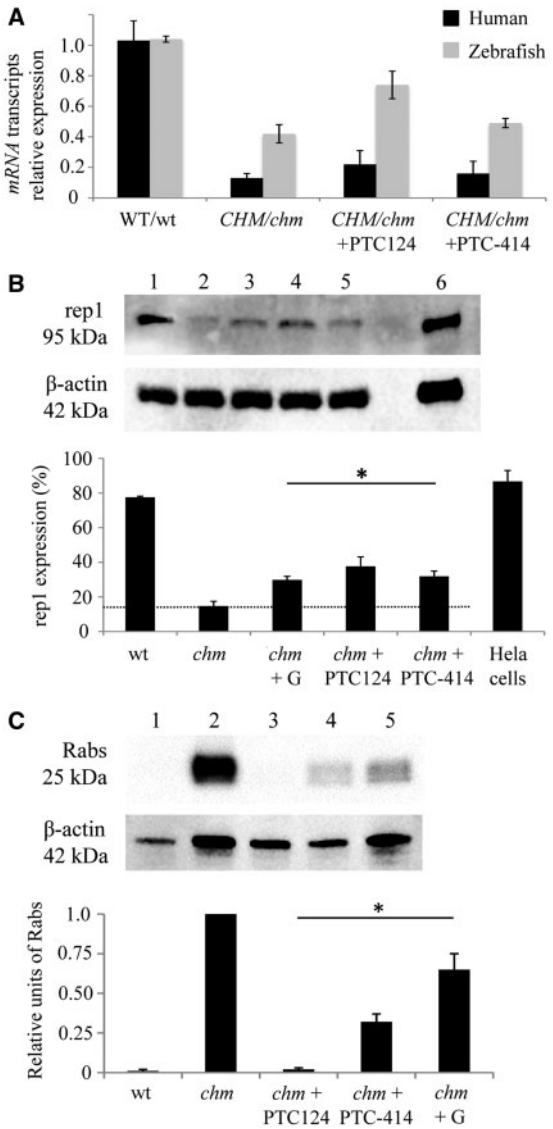

Figure 5. mRNA, protein and prenylation studies. **(A)** Real-time qRT-PCR to detect endogenous full-length mRNA transcripts in human $CHM^{Y42X/y}$ fibroblasts (black bars) and zebrafish chm^{ru848} embryos (grey bars) at 6 dpf (*CHM/chm*) with or without treatment with 40/10 μM PTC124 (+PTC124) or 80 μM/2 μM PTC-414 (+PTC-414) in fibroblasts/zebrafish, respectively, relative to the geometric mean of three internal housekeeping genes (for human *β-2-microglobulin*, *β-tubulin* and *GAPDH*; and for zebrafish *β-actin*, *ribonucleoprotein L13a* and *ef1α*). Values are plotted as the mean ± SEM, $n = 3$. PTC124 significantly increased *chm* mRNA levels compared with untreated mutant zebrafish ($P < 0.01$). This change was not reflected in human *CHM* fibroblasts. **(B)** Western blot analysis of rep1 protein expression. Total zebrafish protein lysates from twenty 6 dpf wt (1), undosed *chm* (2) and mutants treated with 10 μM gentamicin (3), 10 μM PTC124 (4) or 2 μM PTC-414 (5), and positive control Hela cells (6). The blot was stripped and reprobed with anti β-actin as a loading control for samples. Quantification of rep1 protein expression relative to β-actin expression using ImageJ software, represented as mean ± SEM, $n = 3$ independent blots). Dotted line highlights level of maternal rep contribution in untreated *chm* embryos. Increased rep1 protein levels (above the line) were found in all treatment groups representing TRID efficacy. **(C)** *In vitro* prenylation assay showing functional rep1 activity in *chm* mutants treated with TRIDs. Cytosolic extracts from twelve 6 dpf wt (1), undosed *chm* (2), and mutants treated with 10 μM PTC124 (3), 2 μM PTC-414 (4) or 10 μM gentamicin (5) were subjected to *in vitro* prenylation assay using a biotinylated prenyl donor followed by western blot analysis. High signal of incorporated biotin for the undosed *chm* embryos, compared with negligible signal and therefore no accumulation of unprenylated rabs in wt and PTC124 treated embryos, and reduced signal in PTC-414 and gentamicin treatment groups. This result was seen in three independent experimental repeats. The blot was stripped and reprobed with anti β-actin as a loading control for samples.

were analyzed for levels of mRNA transcripts compared with male control wt fibroblasts. $CHM^{Y42X/y}$ fibroblasts expressed a mean 13 ± 3% of wt mRNA levels, and this was comparable to PTC124 (22 ± 9%) and PTC-414 (16 ± 8%) treated $CHM^{Y42X/y}$ patient fibroblasts (Fig. 5A). This is consistent with previous reports of PTC124 having no effect on NMD or other aspects of mRNA stability [9,10].

REP1 protein detection in chm^{ru848} mutants and $CHM^{Y42X/y}$ fibroblasts following TRID treatment

To determine whether PTC124 and PTC-414 treatment increased rep1 protein expression, western blot analysis was undertaken on total zebrafish extracts from wt, untreated and drug-treated chm^{ru848} mutants at 6 dpf. Untreated chm mutants at 6 dpf demonstrated levels of 14.7% rep1 protein expression relative to β-actin, and this source is attributed to residual maternal rep1 derived from the persistent yolk sac. This background maternal contribution was subtracted from the total REP1 detected from treated samples to quantify the amount of protein generated through readthrough. PTC124 and PTC-414-treated chm^{ru848} larvae at 6 dpf expressed a mean increase of 23.1% and 17.2% rep1 protein secondary to nonsense suppression, respectively, after deduction of background maternal contribution (Fig. 5B). Positive control gentamicin showed a 15.1% increase in rep1 protein, suggesting PTC124 has better readthrough efficiency.

Male control WT fibroblasts and patient-derived $CHM^{Y42X/y}$ fibroblasts treated with 50 μM gentamicin, 40 μM PTC124, and 80 μM PTC-414 (concentrations correlated with the maximum prenylation rescue, see below) for a 24-h period were analyzed for REP1 expression by western blotting. No REP1 was detectable by western blot in either the untreated or treated $CHM^{Y42X/y}$ fibroblasts compared with controls (Fig. 6A). The mouse monoclonal anti-REP-1 antibody, clone 2F1 used in this study to detect human REP1 has been extensively characterized and known to detect the 415 C-terminal amino acids of REP1 [11,12].

In vitro prenylation assay

To determine whether the biochemical defect causing CHM was rescued by TRID readthrough, the size of the unprenylated Rab pool was measured using an *in vitro* prenylation assay. Recombinant Rab geranylgeranyl transferase, REP1, and geranyl pyrophosphate (GPP) (the biotinylated prenyl donor) were combined with the lysate of wt or $CHM^{Y42X/y}$ fibroblasts, and whole wt or chm^{ru848} mutant zebrafish. Any unprenylated Rabs available for prenylation, would be labelled with biotin through the prenyl donor and thus be detected by western blot analysis using horseradish peroxidase–conjugated streptavidin [13]. Under these conditions, the semi-quantification of three experiments showed the amount of biotinylated Rab proteins in chm^{ru848} zebrafish extracts reached 100% compared with only 1% in wt extracts (Fig. 5C), and 100% in $CHM^{Y42X/y}$ fibroblasts compared with <1% in wt cells (Fig. 6B-D). Thus, a high level of biotinylated Rabs in chm^{ru848} mutant and $CHM^{Y42X/y}$ fibroblast extracts reflects no REP1 activity in each model system. In fish treated with 10 μM PTC124 or 2 μM PTC-414, the unprenylated Rab pool was reduced by 98 ± 2% and 68 ± 5%, respectively (Fig. 5C). This demonstrated that treatment with both TRIDs resulted in a significantly higher level of functional rep1 activity *in vivo*, compared with untreated fish ($p < 0.01$). In the $CHM^{Y42X/y}$ fibroblasts treated with 50 μM gentamicin (Fig. 6B), 40 μM PTC124 (Fig. 6C) or 80 μM PTC-414 (Fig. 6D) there was a rescue of prenylation

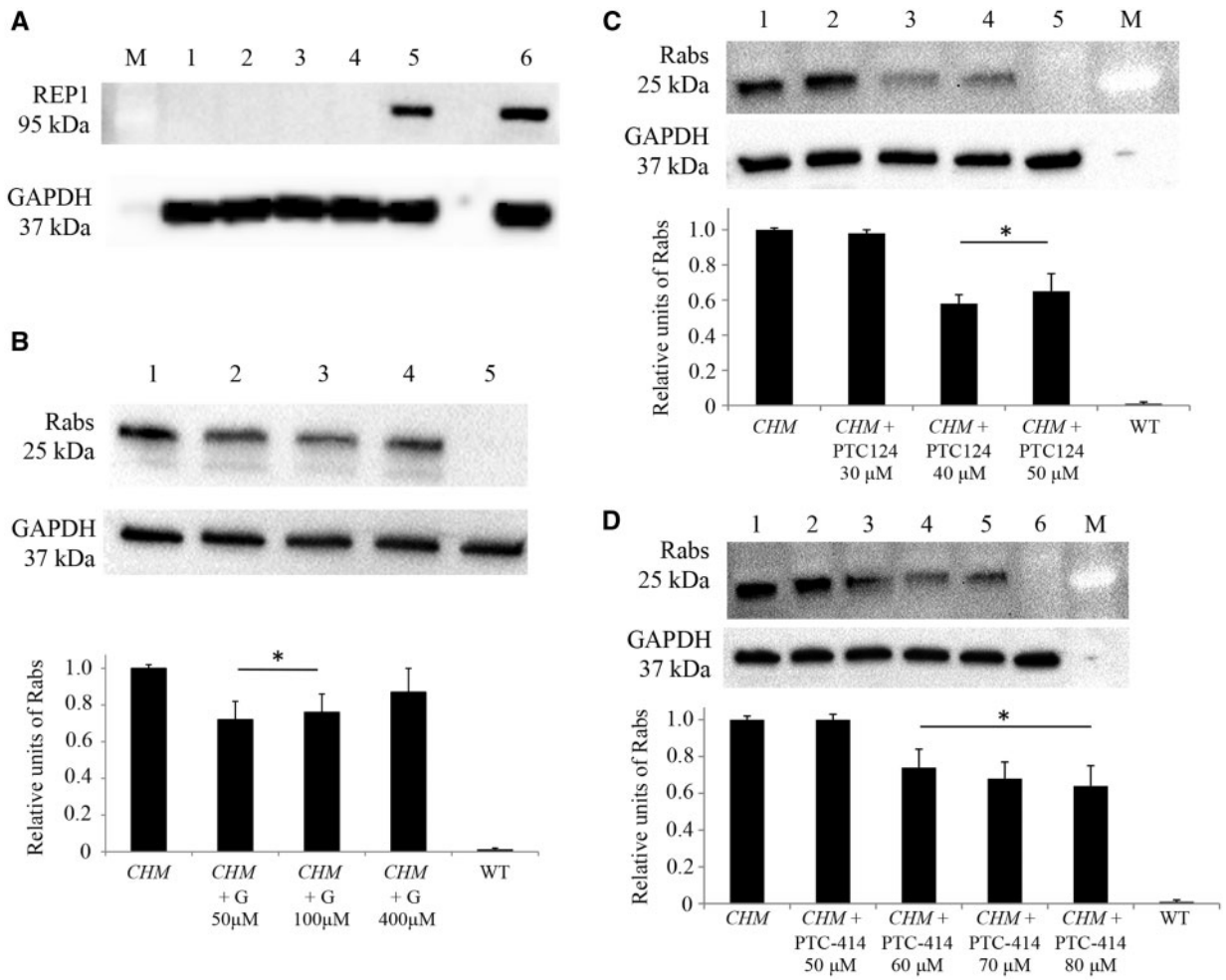

Figure 6. REP1 functional rescue in human *CHM* fibroblasts. **(A)** Western blot analysis of REP1 protein expression showing no detection in untreated $CHM^{Y42X/y}$ fibroblasts (1), or those treated with 50 μM gentamicin (2), 40 μM PTC124 (3) or 80 μM PTC-414 (4). A positive REP1 band was detected in WT fibroblasts (5) and positive control Hela cells (6). The blot was stripped and reprobed with anti-GAPDH as a loading control for samples. This result was seen in three independent experiments. **(B)** *In vitro* prenylation assay showing functional REP1 activity in $CHM^{Y42X/y}$ fibroblasts treated with a range of gentamicin. An unprenylated Rab pool was detected in untreated *CHM* fibroblasts (1). Reducing signal was detected for *CHM* fibroblasts treated with 50 μM (2), 100 μM (3), and 400 μM gentamicin (4). No signal and therefore no accumulation of unprenylated Rabs in the wt control fibroblasts (5). The blot was stripped and reprobed with anti-GAPDH as a loading control for samples. Semi-quantification of the biotinylated Rab pool, after normalization with GAPDH, confirms a significantly lower (*$P < 0.01$) relative quantity of biotinylated Rabs in the *CHM* fibroblasts treated with 50 and 100 μM gentamicin compared with undosed and 400 μM treated cells. Data represented as mean ± SEM, $n = 3$ independent assays. **(C)** *In vitro* prenylation assay showing functional REP1 activity in $CHM^{Y42X/y}$ fibroblasts treated with PTC124. An unprenylated Rab pool was detected in untreated *CHM* fibroblasts (1) and *CHM* fibroblasts treated with 30 μM PTC124 (2). Reducing signal was detected for *CHM* fibroblasts treated with 40 μM PTC124 (3) and 50 μM PTC124 (4), with no signal and therefore no accumulation of unprenylated Rabs in the wt control fibroblasts (5). The blot was stripped and reprobed with anti-GAPDH as a loading control for samples. Semi-quantification of the biotinylated Rab pool, after normalization with GAPDH, confirms a significantly lower (*$P < 0.01$) relative quantity of biotinylated Rabs in the *CHM* fibroblasts treated with ≥40 μM PTC124 compared with undosed and <40 μM treated cells. Data represented as mean ± SEM, $n = 3$ independent assays. **(D)** *In vitro* prenylation assay showing functional REP1 activity in $CHM^{Y42X/y}$ fibroblasts treated with PTC-414. An unprenylated Rab pool was detected in undosed *CHM* fibroblasts (1) and *CHM* fibroblasts treated with 50 μM PTC-414 (2). Reducing signal was detected for *CHM* fibroblasts treated with 60 μM PTC-414 (3), 70 μM PTC-414 (4), and 80 μM PTC-414 (5), with minimal signal in the wt control fibroblasts (6). The blot was stripped and reprobed with anti-GAPDH as a loading control for samples. Semi-quantification of the biotinylated Rab pool, after normalization with GAPDH, confirms a significantly lower (*$P < 0.01$) relative quantity of biotinylated Rabs in the *CHM* fibroblasts treated with ≥60 μM PTC-414 compared with undosed and <50 μM treated cells. Data represented as mean ± SEM, $n = 3$. M, Biorad Precision Plus Dual Colour marker for all blots.

function with 28 ± 10, 42 ± 5 and 36 ± 11% reduction in unprenylated Rab accumulation, respectively.

Discussion

In this study, we have demonstrated that small molecule drugs PTC124 and its derivative PTC-414 can successfully readthrough CHM-related nonsense mutations resulting in functional rescue of REP1 in human derived CHM fibroblasts and arrest of the disease phenotype associated with an overall increase in survival in chm^{ru848} zebrafish. This study provides further evidence that TRIDs have the potential to restore functional protein in patients with retinal disorders and should be translated to clinical trials for those with nonsense-mediated genetic eye disease.

Ataluren (PTC124 or Translarna™) is approved for nonsense mutation Duchenne Muscular Dystrophy (nmDMD) in the EU, exhibiting a good safety profile and clinical benefit in the 6-min walk test in patients when taken orally [14]. This study confirmed that both PTC-derived drugs have a better safety profile than traditional aminoglycosides. PTC124 was found to be safe

and tolerable with negligible effect on renal function and neuromast survival, although PTC-414 did exhibit limited renal toxicity in the zebrafish model.

Treatment of *chm*^{ru848} embryos was optimal at 10 hpf, similar to that in our previous published study examining the translational readthrough effects of gentamicin and paromomycin in ocular coloboma and *chm*^{ru848} zebrafish models [6]. Dosing with 10 μM PTC124 at 3 dpf, prior to the onset of retinal degeneration did not aid the overall survival of the fish, the outcome was found not to be statistically significant. In addition, the dose concentration of PTC124 followed a bell shaped curve in the *chm*^{ru848} mutants treated at 10 hpf, with reduced survival at 5 and 15 μM, comparable to undosed embryos. Studies of aminoglycosides have also manifested bell-shaped dose–response relationships in cells [15–17] and mice [18], and with PTC124 in patients with DMD [19] and the corresponding zebrafish model [20].

The mean baseline levels of mRNA transcripts in *chm*^{ru848} embryos was 42%, indicating a large proportion were escaping NMD, although there is likely to be a significant contribution of normal transcripts from the residual maternal yolk sac at this developmental stage, highlighted by a baseline of 14.7% rep1 protein at 6 dpf in the western blot (Fig. 5B). However, the sensitivity of NMD is multifactorial and a number of molecular mechanisms exist to either trigger or inhibit this process [21,22]. The AUG-proximity effect and translation re-initiation act to suppress NMD [23–25]. This has been demonstrated with human α-globin transcripts, where the boundary of the AUG-proximity effect for NMD resistance resides between codons 30–32, resulting in steady-state levels of between 57 and 95% of wt mRNA levels. [23] Nonsense mutations between codons 32 and 70 in the first half of exon 2 of the human α-globin gene, produced transcript levels ranging from 27 to 40%, indicating full sensitivity to NMD. The AUG-proximity effect is primarily due to the mRNA circulization structure and a short open reading frame (ORF). The nonsense mutation in the *chm*^{ru848} zebrafish model is situated within codon 32 of exon 2, whereas the CHM patient's variant is found within codon 42 of exon 3. Therefore, it is plausible that due to the position of the AUG, an inhibitory NMD effect would account for the higher levels of zebrafish *chm* transcripts. Due to the downstream AUG position in the CHM patient, mRNA transcripts are likely to be susceptible to NMD resulting in the lower baseline levels seen in the fibroblasts.

Translation re-initiation can occur in some genes if an AUG is present 3′ to the PTC, but is dependent on its position, e.g. with human α-globin gene, if the AUG is present at codon 32 following a 5′ PTC, this results in high levels of translation re-initiation [23]. In contrast, an AUG present at codon 55 in the human ß-globin gene failed to inactivate this process. It is unlikely that translation re-initiation will contribute to mRNA levels in CHM, as a second AUG is not present until codon 149 in the *chm* transcript and codon 182 in humans.

Another potential mechanism affecting the levels of mRNA is the presence of an upstream ORF (uORF). This is a regulatory element characterized by an initiation codon in the 5′ UTR that is out-of-frame with the main coding sequence and has a resulting termination codon located upstream or downstream of the main AUG [27]. Bioinformatic studies have shown that ∼49% of the human transcriptome contains uORFs, and these significantly reduce protein expression levels by reducing the efficiency of translation initiation of the main ORF or trigger NMD [28–31]. The human *CHM* transcript has an uORF spanning 18 codons between −20 from the main AUG and a downstream termination codon (TGA) at +32. There is no uORF in the zebrafish *chm* gene. It has been suggested that uORF can trigger NMD as the uORF termination codon can be recognized as premature. Again, due to the circulization of the mRNA transcript, position of the termination codon, and length of the uORF, transcripts with longer uORFs are considered NMD-sensitive compared with those that are shorter [27]. The minimum size of the uORF has not yet been defined in mammalian cells, however studies in plants suggest 35 codons is the threshold [32]. This suggests that the human *CHM* transcripts would be unaffected by this particular NMD trigger. Further work is required to fully understand the NMD pathway response in CHM disease models. By investigating these mechanisms on different nonsense mutations, it may provide a prognostic factor linking treatment response to baseline transcript levels in affected patients. Based on the levels of mRNA transcripts in the disease models, it would be prudent to consider a combination treatment using an NMD inhibitor such as amlexanox together with a TRID to enhance the available substrate for translational readthrough [26].

Previous reports have found that PTC124 does not have any effect on NMD or other aspects of mRNA stability [9,10]. However, from the quantitative RT-PCR results we see higher levels of transcripts in PTC124 dosed *chm*^{ru848} zebrafish compared with the undosed mutants. No significant difference was seen between untreated and treated human *CHM*$^{Y42X/y}$ fibroblasts, showing a more consistent result with previous studies [33]. The exact molecular mechanism of PTC-derived drugs remains unknown, as does nonsense surveillance; both may have differing effects across species that could account for this variation. Nonetheless, having higher baseline mRNA levels is undoubtedly beneficial for translational readthrough therapy as increased substrate will lead to increased protein production [26,34]. From our western blot, rep1 protein levels were detectable in zebrafish extracts but not in human CHM fibroblasts. The human *CHM* uORF may have impacted on protein expression, as uORFs have been found to lower protein levels by 30–80% [29]. Despite this, a marginal amount of REP1, which was not sensitive to detection, must have been produced, as a functional response to treatment with gentamicin, PTC124 and PTC-414 was seen through the biochemical prenylation assay. Others have documented that some readthrough agents have functional benefit in cell or animal systems, but full-length protein cannot be detected due to lack of sensitivity of protein detection assays [35,36]. The proportion of functional rescue was between 1.5–1.7-fold greater than untreated *CHM*$^{Y42X/y}$ fibroblasts. The zebrafish showed 100% prenylation of Rabs with a corresponding 17–23% increase in rep1.

The principle behind translational readthrough therapy is underpinned by mispairing of a near-cognate aminoacyl-tRNA with a stop codon. This occurs at a basal rate of 0.001–0.1% at normal stop codons [37], and 0.01–1% at PTCs [38–40]. One study investigated which amino acids were incorporated into an in-frame UAG PTC near the 5′-end of a ß-galactosidase reporter gene [41]. The resulting full-length protein was subjected to N-terminal sequencing, and revealed that lysine (AAG), tryptophan (UGG) and tyrosine (UAU and UAC), were primarily inserted at the PTC. On the basis that near-cognate mispairing could occur at any of the three positions of the stop codon, predictions of seven amino acid combinations for a UAG stop codon, and six different amino acid codes could be incorporated at either the UAA or UGA codons [42]. In the case of our CHM patient with a p.Y42X (UAG), replacement with tyrosine would successfully restore wt protein. If an alternate amino acid is inserted to introduce a missense protein, this will have little effect on the severity of disease as no genotype-phenotype correlation

has been found in CHM [2,43,44]. However, if increased levels of non-functional full-length protein were formed, the prenylation assay would not have shown any functional rescue.

The results from this study show functional rescue in both zebrafish and human models of CHM, and therefore adds to the evidence that only a small increase in functional protein is enough to prevent the onset or halt/slow progression of recessive disease, notably in retinal degenerations [6]. CHM currently has no effective therapies available. The first Phase I–II viral gene therapy clinical trial involving six patients with CHM was reported to be safe and well tolerated, with a >2- and 4-line improvement in visual acuity in two patients following treatment with the AAV2-REP1 vector [45]. Phase II trials are being planned. TRIDs provide strong potential candidates for a successful pharmacological genetic treatment of CHM. As noted earlier, PTC124 is approved for use in nmDMD in the EU and is in phase III clinical trials for CF (ClinicalTrials.gov Identifier: NCT02107859). Preclinical studies have demonstrated efficacy of PTC124 in a wide range of nonsense mutation-mediated diseases. Previous work by Goldmann and colleagues showed successful readthrough of the p.R31X (UGA) nonsense mutation in *USH1C*, known to cause Usher syndrome type IC, with PTC124 in cell culture, organotypic retina cultures, and *in vivo* mice [46]. Schwarz and colleagues showed production of up to 20% of endogenous, full-length RP2 protein in patient induced pluripotent stem cell derived RPE cells with a p.R120X (UGA) stop codon mutation causing X-linked retinitis pigmentosa [33]. In the aniridia $Pax6^{Sey+/-}$ mouse model with a p.G194X (UGA) nonsense mutation, Gregory-Evans and colleagues showed marked developmental plasticity with post-natal reversal of corneal, lens and retinal malformation defects following treatment with PTC124 [47].

The majority of ocular studies investigating the efficacy of TRIDs were tested on cellular and animal disease models caused by UGA mutations, although UAA nonsense mutations in dystrophin in zebrafish and mice respond to PTC124 treatment. In our paper, we have tested two CHM models with different stop mutations, first human $CHM^{Y42X/y}$ fibroblasts with a UAG, and second, the chm^{ru848} zebrafish with a UAA. PTC-414 was designed to have better potency and readthrough of UAA compounds, consistent with the lower dose of compound associated with an effect. It is important to pursue lead compounds in order to generate an armory of novel small molecule drugs that may differ in their pharmaceutical properties and therefore be preferable for particular genetic conditions for clinical application.

PTC124 and PTC-414 were detectable in the zebrafish following single administration up to day 6. In CHM, the neurosensory retina, RPE and choriocapillaris degenerate relatively independently [4], this leads to a breakdown of the outer blood-retinal-barrier, and hence, should enable orally administered TRIDs to potentially reach the target disease cells. This treatment would not be suitable for individuals who have end-stage disease with extensive chorioretinal atrophy. Postmortem histological sections of a 30-year-old patient with a p.R253X in exon 6 of the *CHM* gene suggested retinal degeneration was observed above either preserved or severely atrophic RPE and choriocapillaris. Patchy islands of relatively well-preserved retinal architecture directly adjacent to areas of severe degeneration [4]. Administration of pharmaceutical agents where retinal cells are present albeit under stress provides the opportunity for generation of functional protein which could help reduce secondary pathological effects like oxidative stress or postpone terminal cell death and improve overall health of the islands of residual retinal tissue.

Interestingly, a recent paper suggests that CHM is a systemic disease as rod- and needle-like crystals have been detected in peripheral blood lymphocytes with significant plasma fatty acid abnormalities [48]. Elevated plasmalogens (which are membrane glycerophospholipids that play a role in the structural properties of cell membranes, including signalling, fission, and fusion, and oxidative stress) [49], and nervonic acid (a monounsaturated omega-9 acid, important in the biosynthesis of neuronal myelin, and found in sphingolipids in the white matter of the human brain) [50], were detected; however the impact in peripheral blood plasma is currently unknown. This crystal deposition is considered to be related to fatty acid dysregulation secondary to defects in REP1-related intracellular vesicular trafficking. A systemic treatment, such as PTC124, therefore has the potential to prevent multisystem crystalline inclusion deposition and normalize any lipid disequilibrium. Detailed longitudinal clinical phenotyping studies are underway for CHM to understand the natural history of the disease and identify the most suitable therapeutic window. Clinical trials with Ataluren are forthcoming and may provide a potential treatment for those patients with CHM, but also associated inherited retinal disorders.

Materials and Methods

The study protocol adhered to the tenets of the Declaration of Helsinki and received approval from the NRES Committee London-Riverside Ethics Committee (REC12/LO/0489). Written, informed consent was obtained from all participants prior to their inclusion in this study. Zebrafish (wt AB and chm^{ru848}) were bred and maintained in the University College London animal facility according to standard protocols and the guidelines of the ARVO Statement for the Use of Animals in Ophthalmic and Vision Research [51].

Zebrafish husbandry

wt AB (wt) and chm^{ru848} embryos were generated by natural pair-wise matings of identified heterozygous carriers and raised at 28.5 °C on a 14-h light/10-h dark cycle in a 100 mm^2 petri dish containing aquarium water. The developmental stages are given in hours/days post-fertilization (hpf/dpf), according to morphological criteria [52].

Cell culture of fibroblasts from skin biopsies

A 5 mm punch skin biopsy was obtained from a 25-year-old CHM patient (genotype confirmed p.Y42X [UAG] in exon 3) and an age-matched healthy male control under local anaesthetic. The biopsies were sectioned into smaller (1 mm) pieces using sterile scalpel blades and placed into a 6-well plate. The tissue was exposed to a minimal amount of fibroblast growth media (DMEM, 10% foetal calf serum, 1 mM non-essential amino acids, 1 mM GlutaMAX™ and penicillin–streptomycin, Life Technologies, Germany), overlaid with a sterile coverslip overnight and incubated at 37°C in 5% CO_2 in a humidified incubator. The following day 2 ml of fresh medium was added. The tissue was cultured until sufficient fibroblast outgrowth had occurred (~4 weeks) for further passage of cells. Fibroblast cells were washed in PBS, dissociated using TrypLE Express (Life Technologies, Germany) and re-plated at a split ratio of 1:3. For maintenance, the media was replaced every 2–3 days and cells passaged when 80–90% confluent. Genomic DNA was extracted

from fibroblast cells using the GeneEuteTM Mammalian Genomic DNA miniprep Kit (Sigma) and used in direct sequencing to re-confirm the *CHM* mutation.

Drug efficacy

Dechorionated wt embryos at 10 hpf were treated with test compounds, range from 0.025 to 40 μM; PTC124 (SelleckChem), PTC-414 (PTC Therapeutics Inc.) and gentamicin (Sigma, solution of 50 mg/ml in deionized water, liquid, sterile-filtered, BioReagent). Drugs were directly added to the aquaria water and embryos were raised until 6 dpf. For each treatment, 30 embryos were used and three independent experiments were performed. Outcomes were based on mortality and tolerability effects including behavioural and morphological defects at 6 dpf. Embryos surviving to 6 dpf with no signs of toxicity were prepared for histological analysis of the retina, ototoxicity studies (through neuromast survival and immunostaining) and renal function assays to determine tolerability.

Levels of PTC124 and PTC-414 were measured in wt embryos at days 1, 3 and 6 post-single dose of 10 μM PTC124 and 2 μM of PTC-414 at 10 hpf to measure the concentration of compound within the whole embryo. Twenty embryos per group were analyzed; three independent experiments performed. Embryos were homogenized and then mixed with acetonitrile-methanol mixture containing an internal standard that is a close analog of the test compounds. The samples were centrifuged and the supernatant was collected and quantified using electro-spray liquid chromatography-tandem mass spectrometry (LC-MS/MS).

Fibroblasts were seeded at 600 000 cells per well of a six-well plate (Fisher Scientific, UK) and allowed to adhere for 24 h. Cells were subsequently dosed twice over 24 h with gentamicin, PTC124 and PTC-414 (concentration range from 50–400, 30–60 and 50–80 μM, respectively) in DMEM + 10% FBS in the absence of any antibiotics. Compound was added to cells at 24 h after seeding, and again after a further 8 h. Cells were sampled 24 h after the initial compound addition.

PTC124 and PTC-414 survival studies

The *chm*^{ru848} mutant embryos were dechorionated at 10 hpf and treated with either 10 μM of PTC124, 2 μM of PTC-414, 10 μM of gentamicin as a positive control or kept in control (drug-free) aquaria water. Survival of mutant larvae was recorded in days, $n = 50$ for each treatment group. Further experiments using 5 and 15 μM of PTC124 were tested on *chm*^{ru848} embryos to confirm that the optimum dose for this study was 10 μM on the basis of initial survival experiments. *chm*^{ru848} embryos were also dosed with 10 μM PTC124 and 2 μM PTC-414 at 3 dpf and their survival observed.

Retinal histology and morphological studies

At 6 and 10 dpf, embryos from each treatment group were collected and fixed in 4% paraformaldehyde (PFA) overnight at 4°C. They were dehydrated through a graded ethanol series and then embedded in JB-4 plastic resin (Polysciences/Sigma) according to the manufacturer's instructions [53]. A Leica 2065 microtome was used to cut 7 μm sections, which were mounted on Polytetrafluoroethylene multi-well printed microscope slides, stained with 1% Toluidine Blue and sealed with DPX mountant (Fisher) and 20 × 50 mm cover glass (VWR). Retinal histology was imaged using a Leica DMRB with Jenoptik D-07739 Optical System and wholemount images for morphological analysis were taken with a Nikon SMZ-1500 stereo microscope with Nikon Digital Sight DS-Fi2 system.

TUNEL assay

Five embryos at 6 dpf from each treatment group were collected and fixed in 4% PFA overnight at 4°C. The embryos were then cryoprotected in 30% sucrose for 4 h and embedded in Tissue-Tek® OCT™ and frozen on dry ice. Retinal sections were cut at 12 μm thickness using a Leica CM1850 Cryostat and mounted on Superfrost Plus slides. Following the manufacturer's instructions, the ApopTag Fluorescein In Situ Apoptosis Detection Kit (Millipore) was used to detect levels of apoptotic cell death. Sections were counterstained and sealed with Prolong Diamond Antifade Mountant + DAPI (Life Technologies). Levels of fluorescence from apoptotic cell death were imaged using a Zeiss LSM510 upright confocal microscope, stacked images were analyzed using ImageJ.

DHE staining

Levels of oxidative stress, generated through the presence of superoxide in the cytoplasm of cells, were detected in the eyes of live embryos using dihydroethidium (DHE, Life Technologies) [54]. Five embryos at 6 dpf from each treatment group were incubated at 37°C for 5 min in 3 μM DHE. The embryos were washed twice with sterile water and then orientated and mounted in methylcellulose on multi-well microscope slides. Levels of red fluorescence present in the whole eye due to the oxidation of DHE was imaged using a Zeiss LSM510 upright confocal microscope, stacked images were analyzed using ImageJ.

Neuromast hair cell staining for ototoxicity

Five wt embryos at 6 dpf from each treatment group were collected and incubated in 200 μM 4-(4-diethylaminostyryl)-N-methylpyridinium iodide (4-Di-2-Asp, Sigma) for 1 min at room temperature. The embryos were then orientated and mounted in methyl cellulose on self-made multiwell microscope slides and fluorescent signal from neuromasts was imaged using a Zeiss LSM510 upright confocal microscope and analyzed using a modified neuromast scoring system [7,55]. Zebrafish larvae have 19 head neuromasts on each side that contribute to the lateral line system and were used as a scoring template for neuromast hair cell survival in $n = 5$ per treatment group (Fig. 2C). Individual neuromasts were scored as having normal 4-Di-2-Asp staining indicating hair cells are present (score = 2), reduced staining (score = 1) or absent staining (score = 0). Total neuromast scores were measured only the left side of each fish. The maximum score possible was 38 (19 multiplied by the high score of 2), which indicates normal staining of each neuromast.

To assess more detailed information about the number of hair cells present in an individual neuromast, embryos at 6 dpf were blocked in PBS with 1% Triton-X and 20% normal goat serum (ngs) (both Sigma) for 4 h at room temperature and then underwent wholemount immunostaining with anti-acetylated tubulin (Sigma) diluted 1:500 in PBS with 0.5% Triton-X and 1% normal goat serum (ngs) overnight at 4°C. Embryos were then incubated for 1 h at room temperature with Alexa Fluor 488 secondary antibody (Life Technologies) diluted 1:10000 in PBS with 0.5% Triton-X and 1% ngs and then counterstained with Alexa Fluor 647 Phalloidin (Life Technologies) diluted 1:10 in PBS with

0.5% Triton-X and 1% ngs. The embryos were then orientated and mounted in 1% agarose on self-made multiwell microscope slides and sealed using DPX mountant (Fisher) with 20 × 50 mm cover glass (VWR). Fluorescent hair cells were visualized using Zeiss LSM710 AxioImage M.1 upright confocal microscope. The number of hair cells in the OP neuromast was counted as a further representation of drug toxicity.

Fluorescent clearance assay for renal function

Pronephric tubule filtration efficiency of 5 wt embryos from each treatment group was detected using pericardial microinjections of rhodamine dextran (Life technologies) [56]. Using a Picospritzer III (Parker Instruments) and Narashige micromanipulator (Intracel), 1 nl of 5 mg/ml rhodamine-labelled 10 kDa dextran (Life Technologies) was injected into the pericardial cavity of live 3 dpf embryos. At 4 and 24 h post-injection, the embryos were orientated and mounted on a multi-well microscope slide and fluorescent signal from the presence of rhodamine dextran was imaged using a Zeiss LSM510 upright confocal microscope and analyzed using ImageJ.

RT-qPCR

To determine the level of *CHM*/*chm* transcript, in order to relate this to the efficiency of the TRIDs treatment, total RNA was extracted from 6 dpf wt, chm^{ru848} zebrafish, human $CHM^{+/y}$ and $CHM^{Y42X/y}$ fibroblasts (TRID treated and untreated) using the RNeasy micro kit (Qiagen, UK) according to the manufacturer's instructions. Using 500 ng total RNA, cDNA was reverse transcribed using a Superscript III First-strand synthesis Supermix kit (Life Technologies). For quantitative real-time PCR amplifications, gene expression was quantified using SYBR Select fluorescent dye (Life Technologies) in triplicate reactions for each sample. All RT-qPCR primers and conditions are listed in Table 2.

Zebrafish *chm* transcripts were amplified from exon 14 to exon 15 using intronic spanning primers with expression normalized to the geometric mean of *β-actin*, *ribonucleoprotein L13a* and *ef1α* internal housekeeping genes. Similarly, human *CHM* transcripts were amplified from exon 14 to exon 15 using intronic spanning primers and expression normalized to the geometric mean of human *β-2-microglobulin*, *β-tubulin* and *GAPDH* internal housekeeping genes. The StepOne Plus RealTime PCR System (Life Technologies) was used and reactions analyzed using the Comparative C_T experiment option in the StepOne software (Version 2.3).

Table 2. Genotyping PCR and qRT-PCR primers with conditions for the amplification of zebrafish *chm*, human *CHM* and housekeeping genes

Gene Primers	Annealing (°C)	Size (bp)
Zebrafish *chm* forward primer ACCATGGGCCGCCACCATGGC TGCGGAGGATCTCCCGTCT	60	496
Zebrafish *chm* reverse primer TCCATGGGCGCAGAATCTTCATTCTCTTC		
Human *CHM* forward primer ACAAACTCCAAGCAGCGATCCA	57	370
Human *CHM* reverse primer TGCTCTGGAACACGGAACCTG		
Zebrafish *chm* qPCR forward primer TGGACTGGGCAGCGACTACT	60	134
Zebrafish *chm* qPCR forward primer CTTCAGCCTGTGGAGCGTCA		
Zebrafish *β-actin* qPCR reverse primer TGTACCCTGGCATTGCTGAC	60	144
Zebrafish *β-actin* qPCR reverse primer TGGAAGGTGGACAGGGAGGC		
Zebrafish *ribonucleoprotein L13a* qPCR forward primer TCTGGAGGACTGTAAGAGGTATGC	60	148
Zebrafish *ribonucleoprotein L13a* qPCR reverse primer AGACGCACAATCTTGAGAGCAG		
Zebrafish *ef1α* qPCR forward primer CTGGAGGCCAGCTCAAACAT	60	87
Zebrafish *ef1α* qPCR reverse primer ATCAAGAAGAGTAGTACCGCTAGCATTAC		
Human *CHM* qPCR forward primer TGGACTGGGCAGCGACTACT	60	163
Human *CHM* qPCR reverse primer CTTCAGCCTGTGGAGCGTCA		
Human *β2-microglobulin* forward primer TGTACCCTGGCATTGCTGAC	60	97
Human *β2- microglobulin* reverse primer TGGAAGGTGGACAGGGAGGC		
Human *β-tubulin* forward primer TCTGGAGGACTGTAAGAGGTATGC	60	119
Human *β-tubulin* reverse primer AGACGCACAATCTTGAGAGCAG		
Human *GAPDH* forward primer CTGGAGGCCAGCTCAAACAT	60	104
Human *GAPDH* reverse primer ATCAAGAAGAGTAGTACCGCTAGCATTAC		

Western blotting

Protein was isolated from 20 embryos per treatment condition at 6 dpf: wt, untreated chm^{ru848} and mutants treated with 10 μM PTC124, 2 μM PTC-414 and 10 μM gentamicin. Embryos were snap-frozen in liquid nitrogen and homogenized by sonication (3 × 10 s, XL-2000 Qsonica LLC) with cold RIPA lysis buffer (Pierce) containing 1x Protease Inhibitor Cocktail (Sigma) and 1× Phosphatase Inhibitor Cocktail (Pierce).

Patient CHM fibroblasts were seeded in DMEM containing 10% FBS with no antibiotics at 600 000 cells per well of a 6-well tissue culture plate and allowed to attach to the plate for 24 h. Cells were subsequently treated with 50 μM gentamicin, 40 μM PTC124 and 80 μM PTC-414 for a further 24 h period before being collected for western blot. Cells were washed 1X ice-cold PBS and lysed on ice in a buffer containing: 10mM HEPES, 1% Triton, 150mM KCL, 1mM PMSF, 10 ng/ml leupeptin, 1 mM DTT, 50 ng/ml aprotinin, 10 mM NaF and 100 μM sodium vanadate. Lysed cells were transferred to a microcentrifuge tube and incubated at 4 °C for 30 min. Cell debris was removed by centrifugation at 13 000 rpm for 30 min at 4 °C.

Protein concentration was measured using the BCA Protein Assay Kit (Pierce), a plate reader (Tecan Safire) and Magellan Software. For each sample, 30 μg of protein was boiled at 95 °C for 5 min with 5 μl Nupage sample buffer and 2μl Nupage reducing agent (Life Technologies). Proteins were separated on an Any kD SDS–polyacrylamide gel (BioRad) and transferred onto an Immun-Blot PVDF membrane (BioRad). The membrane was blocked overnight at 4°C in blocking solution [5% dry milk, PBS/

0.4% Tween (PBST)], washed five times in PBST and then incubated for 2 h at room temperature with 1:1000 primary anti-Rep J905 antibody for the zebrafish extract [6], and 1:500 2F1 antibody (Millipore) for the human fibroblasts [54]. Following five washes in PBST, the membrane was incubated with 1:10 000 secondary anti-rabbit IgG HRP conjugate (Sigma) in 1% milk-PBST for 1 h at room temperature. The membrane was washed five times in PBST before chemiluminescent detection using the ECL Prime Western Blotting Detection Kit (GE Healthcare) and the ChemiDoc MP Imaging system (Biorad). Using Restore Western Blot Stripping Buffer (Pierce), the membrane was stripped and re-probed with 1:5000 polyclonal anti-β-actin antibody (Sigma) as a loading control for both zebrafish and human fibroblasts. ImageLab software (BioRad) was used to determine the relative abundance of REP1/rep1 protein compared with corresponding levels of control protein expression. Three independent experiments were performed to determine the mean protein expression.

In vitro prenylation assay

Twelve embryos per treatment condition at 6 dpf were used: wt, untreated *chm*^{ru848} and treated *chm*^{ru848} with 10 μM PTC124, 2 μM PTC-414 or 10 μM gentamicin. Embryos were snap-frozen in liquid nitrogen and then homogenized in cold, degassed buffer (25 mM HEPES pH 7.2, 50 mM NaCl, 1 mM $MgCl_2$, 2mM DTE, 1× Protease Inhibitor Cocktail) by sonication (3× 10 s, XL-2000 Qsonica LLC). Nuclei were pelleted by centrifugation at 1500 g for 5 min at 4 °C, then the post-nuclear supernatant was collected and centrifuged at 100 000g for 1 h at 4 °C using a TLA45 rotor in a Optima MAX-E Beckman Coulter to obtain cytosolic protein extracts.

Human *CHM* fibroblasts, untreated and treated with an increasing concentration of gentamicin (up to 400 μM), PTC124 (up to 50 μM) or PTC-414 (up to 80 μM), cultured in a 6-well plate were washed in cold PBS, scraped in PBS containing antiproteases, pelleted and resuspended in cold, degassed prenylation/lysis buffer prepared fresh as described previously in [57]. Cells were incubated 15 min on ice and then sonicated three times for 45 s at 40 Hz. The cells were then centrifuged for 5 min at 1500 g at 4 °C, the supernatant collected and further centrifuged for 1 h at 50 000 g at 4 °C on an Optima MAX-TL ultracentrifuge (Beckman, France).

An *in vitro* prenylation assay was performed on the freshly prepared lysate using 5 μM biotin-labelled geranyl pyrophosphate (B-GPP) (Jena Bioscience, Germany) as a prenyl group donor, 0.5 μM recombinant REP1 (Jena Bioscience, Germany), 0.5 μM recombinant Rab geranylgeranyl transferase (RGGT; Jena Bioscience, Germany) and 20 μM GDP in prenylation/lysis buffer at 37 °C for 1 h [13,57,58]. The prenylation reaction was stopped with 6× SDS loading buffer, boiled at 95 °C for 5 min and biotin incorporation analyzed by western blot. The membrane was incubated with 1:3000 HRP-conjugated streptavidin (Jackson ImmunoResearch, Cambridge, Great Britain) and 1:2000 goat anti GAPDH (Everest Biotech Ltd., UK). Detection was performed using the ChemiDoc MP Imaging system (Biorad). The amount of biotinylated Rab proteins was then quantified by scanning densitometry using the appropriate software package (ImageJ) and expressed as a function of the GAPDH signal. To allow relative comparisons, the biotinylated Rab population in the untreated CHM samples was set to 100%. Three independent experiments were performed to determine the mean prenylation function following drug treatment.

Statistical analysis

All results are expressed as mean ± SEM, unless specified. As sample sizes are small, non-parametric tests were used. Differences between control untreated and each treatment group were assessed by pair-wise comparisons using the Mann-Whitney test or the Kruskal–Wallis analysis of variance if more than two groups were investigated, followed by Dunn's multiple comparison test where appropriate. A P-value of <0.01 was considered statistically significant.

Acknowledgements

Our thanks extend to Professor A. James Hudspeth from the Howard Hughes Medical Institute, Rockefeller University, New York, USA, for kindly donating the *chm*^{ru848} zebrafish line. The authors thank Shirley Yeh from PTC Therapeutics for bioanalytical support. We gratefully acknowledge the support of the National Institute for Health Research (NIHR) Biomedical Research Centre based at Moorfields Eye Hospital NHS Foundation Trust and UCL Institute of Ophthalmology.

Conflict of Interest statement. Ellen Welch and Marla Weetall are financially compensated as employees of PTC Therapeutics. No other author has any conflict of interest.

Funding

Funding received from the Choroideremia Research Foundation US, France Choroideremia, Fight for Sight UK and Moorfields Eye Charity. The research leading to these results has received funding from the European Union Seventh Framework Programme [FP7-People-2012-ITN] under grant agreement 317472 (EyeTN).

References

1. Seabra, M.C., Mules, E.H. and Hume, A.N. (2002) Rab GTPases, intracellular traffic and disease. *Trends Mol. Med.*, **8**, 23–30.
2. Moosajee, M., Ramsden, S.C., Black, G.C., Seabra, M.C. and Webster, A.R. (2014) Clinical utility gene card for: choroideremia. *Eur. J. Hum. Genet.*, **22**, doi: 10.1038/ejhg.2013.183.
3. Rak, A., Pylypenko, O., Niculae, A., Pyatkov, K., Goody, R.S. and Alexandrov, K. (2004) Structure of the Rab7:REP-1 complex: insights into the mechanism of Rab prenylation and choroideremia disease. *Cell*, **117**, 749–760.
4. MacDonald, I.M., Russell, L. and Chan, C.C. (2009) Choroideremia: new findings from ocular pathology and review of recent literature. *Surv. Ophthalmol.*, **54**, 401–407.
5. Moosajee, M., Tulloch, M., Baron, R.A., Gregory-Evans, C.Y., Pereira-Leal, J.B. and Seabra, M.C. (2009) Single choroideremia gene in nonmammalian vertebrates explains early embryonic lethality of the zebrafish model of choroideremia. *Invest. Ophthalmol. Vis. Sci.*, **50**, 3009–3016.
6. Moosajee, M., Gregory-Evans, K., Ellis, C.D., Seabra, M.C. and Gregory-Evans, C.Y. (2008) Translational bypass of nonsense mutations in zebrafish rep1, pax2.1 and lamb1 highlights a viable therapeutic option for untreatable genetic eye disease. *Hum. Mol. Genet.*, **17**, 3987–4000.
7. Harris, J.A., Cheng, A.G., Cunningham, L.L., MacDonald, G., Raible, D.W. and Rubel, E.W. (2003) Neomycin-induced hair cell death and rapid regeneration in the lateral line of zebrafish (Danio rerio). *J. Assoc. Res. Otolaryngol.*, **4**, 219–234.

8. Sha, S.H. and Schacht, J. (1999) Formation of reactive oxygen species following bioactivation of gentamicin. *Free Radic. Biol. Med.*, **26**, 341–347.
9. Du, M., Liu, X., Welch, E.M., Hirawat, S., Peltz, S.W. and Bedwell, D.M. (2008) PTC124 is an orally bioavailable compound that promotes suppression of the human CFTR-G542X nonsense allele in a CF mouse model. *Proc. Natl. Acad. Sci. U S A*, **105**, 2064–2069.
10. Welch, E.M., Barton, E.R., Zhuo, J., Tomizawa, Y., Friesen, W.J., Trifillis, P., Paushkin, S., Patel, M., Trotta, C.R., Hwang, S. *et al.* (2007) PTC124 targets genetic disorders caused by nonsense mutations. *Nature*, **447**, 87–91.
11. Alexandrov, K., Horiuchi, H., Steele-Mortimer, O., Seabra, M.C. and Zerial, M. (1994) Rab escort protein-1 is a multifunctional protein that accompanies newly prenylated rab proteins to their target membranes. *Embo J*, **13**, 5262–5273.
12. MacDonald, I.M., Mah, D.Y., Ho, Y.K., Lewis, R.A. and Seabra, M.C. (1998) A practical diagnostic test for choroideremia. *Ophthalmology*, **105**, 1637–1640.
13. Cereso, N., Pequignot, M.O., Robert, L., Becker, F., De Luca, V., Nabholz, N., Rigau, V., De Vos, J., Hamel, C.P. and Kalatzis, V. (2014) Proof of concept for AAV2/5-mediated gene therapy in iPSC-derived retinal pigment epithelium of a choroideremia patient. *Mol. Ther. Methods Clin. Dev.*, **1**, 14011.
14. Hirawat, S., Welch, E.M., Elfring, G.L., Northcutt, V.J., Paushkin, S., Hwang, S., Leonard, E.M., Almstead, N.G., Ju, W., Peltz, S.W., *et al.* (2007) Safety, tolerability, and pharmacokinetics of PTC124, a nonaminoglycoside nonsense mutation suppressor, following single- and multiple-dose administration to healthy male and female adult volunteers. *J. Clin. Pharmacol.*, **47**, 430–444.
15. Burke, J.F. and Mogg, A.E. (1985) Suppression of a nonsense mutation in mammalian cells in vivo by the aminoglycoside antibiotics G-418 and paromomycin. *Nucleic Acids Res.*, **13**, 6265–6272.
16. Lai, C.H., Chun, H.H., Nahas, S.A., Mitui, M., Gamo, K.M., Du, L. and Gatti, R.A. (2004) Correction of ATM gene function by aminoglycoside-induced read-through of premature termination codons. *Proc. Natl. Acad. Sci. U S A*, **101**, 15676–15681.
17. Bellais, S., Le Goff, C., Dagoneau, N., Munnich, A. and Cormier-Daire, V. (2009) In vitro readthrough of termination codons by gentamycin in the Stuve-Wiedemann Syndrome. *Eur. J. Hum. Genet.*, **18**, 130–132.
18. Yang, C., Feng, J., Song, W., Wang, J., Tsai, B., Zhang, Y., Scaringe, W.A., Hill, K.A., Margaritis, P., High, K.A. *et al.* (2007) A mouse model for nonsense mutation bypass therapy shows a dramatic multiday response to geneticin. *Proc. Natl. Acad. Sci. U S A*, **104**, 15394–15399.
19. Bushby, K., Finkel, R., Wong, B., Barohn, R., Campbell, C., Comi, G.P., Connolly, A.M., Day, J.W., Flanigan, K.M., Goemans, N. *et al.* (2014) Ataluren treatment of patients with nonsense mutation dystrophinopathy. *Musc. Nerve*, **50**, 477–487.
20. Li, M., Andersson-Lendahl, M., Sejersen, T. and Arner, A. (2013) Muscle dysfunction and structural defects of dystrophin-null sapje mutant zebrafish larvae are rescued by ataluren treatment. *FASEB J.*, **28**, 1593–1599.
21. Amrani, N., Ganesan, R., Kervestin, S., Mangus, D.A., Ghosh, S. and Jacobson, A. (2004) A faux 3'-UTR promotes aberrant termination and triggers nonsense-mediated mRNA decay. *Nature*, **432**, 112–118.
22. Le Hir, H., Gatfield, D., Izaurralde, E. and Moore, M.J. (2001) The exon-exon junction complex provides a binding platform for factors involved in mRNA export and nonsense-mediated mRNA decay. *Embo J.*, **20**, 4987–4997.
23. Pereira, F.J., Teixeira, A., Kong, J., Barbosa, C., Silva, A.L., Marques-Ramos, A., Liebhaber, S.A. and Romao, L. (2015) Resistance of mRNAs with AUG-proximal nonsense mutations to nonsense-mediated decay reflects variables of mRNA structure and translational activity. *Nucleic Acids Res.*, **43**, 6528–6544.
24. Romao, L., Inacio, A., Santos, S., Avila, M., Faustino, P., Pacheco, P. and Lavinha, J. (2000) Nonsense mutations in the human beta-globin gene lead to unexpected levels of cytoplasmic mRNA accumulation. *Blood*, **96**, 2895–2901.
25. Silva, A.L., Ribeiro, P., Inacio, A., Liebhaber, S.A. and Romao, L. (2008) Proximity of the poly(A)-binding protein to a premature termination codon inhibits mammalian nonsense-mediated mRNA decay. *RNA*, **14**, 563–576.
26. Gonzalez-Hilarion, S., Beghyn, T., Jia, J., Debreuck, N., Berte, G., Mamchaoui, K., Mouly, V., Gruenert, D.C., Deprez, B. and Lejeune, F. (2012) Rescue of nonsense mutations by amlexanox in human cells. *Orphanet. J. Rare Dis.*, **7**, 58.
27. Barbosa, C., Peixeiro, I. and Romao, L. (2013) Gene expression regulation by upstream open reading frames and human disease. *PLoS Genet.*, **9**, e1003529.
28. Morris, D.R. and Geballe, A.P. (2000) Upstream open reading frames as regulators of mRNA translation. *Mol. Cell. Biol.*, **20**, 8635–8642.
29. Calvo, S.E., Pagliarini, D.J. and Mootha, V.K. (2009) Upstream open reading frames cause widespread reduction of protein expression and are polymorphic among humans. *Proc. Natl. Acad. Sci. U S A*, **106**, 7507–7512.
30. Yepiskoposyan, H., Aeschimann, F., Nilsson, D., Okoniewski, M. and Muhlemann, O. (2011) Autoregulation of the nonsense-mediated mRNA decay pathway in human cells. *RNA*, **17**, 2108–2118.
31. Ye, Y., Liang, Y., Yu, Q., Hu, L., Li, H., Zhang, Z. and Xu, X. (2015) Analysis of human upstream open reading frames and impact on gene expression. *Hum. Genet.*, **134**, 605–612.
32. Nyiko, T., Sonkoly, B., Merai, Z., Benkovics, A.H. and Silhavy, D. (2009) Plant upstream ORFs can trigger nonsense-mediated mRNA decay in a size-dependent manner. *Plant Mol. Biol.*, **71**, 367–378.
33. Schwarz, N., Carr, A.J., Lane, A., Moeller, F., Chen, L.L., Aguila, M., Nommiste, B., Muthiah, M.N., Kanuga, N., Wolfrum, U. *et al.* (2015) Translational read-through of the RP2 Arg120stop mutation in patient iPSC-derived retinal pigment epithelium cells. *Hum. Mol. Genet.*, **24**, 972–986.
34. Linde, L., Boelz, S., Nissim-Rafinia, M., Oren, Y.S., Wilschanski, M., Yaacov, Y., Virgilis, D., Neu-Yilik, G., Kulozik, A.E., Kerem, E. *et al.* (2007) Nonsense-mediated mRNA decay affects nonsense transcript levels and governs response of cystic fibrosis patients to gentamicin. *J. Clin. Invest.*, **117**, 683–692.
35. Wang, D., Belakhov, V., Kandasamy, J., Baasov, T., Li, S.C., Li, Y.T., Bedwell, D.M. and Keeling, K.M. (2011) The designer aminoglycoside NB84 significantly reduces glycosaminoglycan accumulation associated with MPS I-H in the Idua-W392X mouse. *Mol. Genet. Metab.*, **105**, 116–125.
36. Sarkar, C., Zhang, Z. and Mukherjee, A.B. (2011) Stop codon read-through with PTC124 induces palmitoyl-protein thioesterase-1 activity, reduces thioester load and suppresses apoptosis in cultured cells from INCL patients. *Mol. Genet. Metab.*, **104**, 338–345.
37. Parker, J. (1989) Errors and alternatives in reading the universal genetic code. *Microbiol. Rev.*, **53**, 273–298.

38. Bonetti, B., Fu, L., Moon, J. and Bedwell, D.M. (1995) The efficiency of translation termination is determined by a synergistic interplay between upstream and downstream sequences in Saccharomyces cerevisiae. *J. Mol. Biol.*, **251**, 334–345.
39. Cassan, M. and Rousset, J.P. (2001) UAG readthrough in mammalian cells: effect of upstream and downstream stop codon contexts reveal different signals. *BMC Mol. Biol.*, **2**, 3.
40. Manuvakhova, M., Keeling, K. and Bedwell, D.M. (2000) Aminoglycoside antibiotics mediate context-dependent suppression of termination codons in a mammalian translation system. *RNA*, **6**, 1044–1055.
41. Fearon, K., McClendon, V., Bonetti, B. and Bedwell, D.M. (1994) Premature translation termination mutations are efficiently suppressed in a highly conserved region of yeast Ste6p, a member of the ATP-binding cassette (ABC) transporter family. *J. Biol. Chem.*, **269**, 17802–17808.
42. Keeling, K.M., Wang, D., Conard, S.E. and Bedwell, D.M. (2012) Suppression of premature termination codons as a therapeutic approach. *Crit. Rev. Biochem. Mol. Biol.*, **47**, 444–463.
43. Sergeev, Y.V., Smaoui, N., Sui, R., Stiles, D., Gordiyenko, N., Strunnikova, N. and Macdonald, I.M. (2009) The functional effect of pathogenic mutations in Rab escort protein 1. *Mutat. Res.*, **665**, 44–50.
44. Esposito, G., De Falco, F., Tinto, N., Testa, F., Vitagliano, L., Tandurella, I.C., Iannone, L., Rossi, S., Rinaldi, E., Simonelli, F. *et al.* (2011) Comprehensive mutation analysis (20 families) of the choroideremia gene reveals a missense variant that prevents the binding of REP1 with Rab geranylgeranyl transferase. *Hum. Mutat.*, **32**, 1460–1469.
45. MacLaren, R.E., Groppe, M., Barnard, A.R., Cottriall, C.L., Tolmachova, T., Seymour, L., Clark, K.R., During, M.J., Cremers, F.P., Black, G.C. *et al.* (2014) Retinal gene therapy in patients with choroideremia: initial findings from a phase 1/2 clinical trial. *Lancet*, **383**, 1129–1137.
46. Goldmann, T., Overlack, N., Wolfrum, U. and Nagel-Wolfrum, K. (2011) PTC124-mediated translational readthrough of a nonsense mutation causing Usher syndrome type 1C. *Hum. Gene Ther.*, **22**, 537–547.
47. Gregory-Evans, C.Y., Wang, X., Wasan, K.M., Zhao, J., Metcalfe, A.L. and Gregory-Evans, K. (2013) Postnatal manipulation of Pax6 dosage reverses congenital tissue malformation defects. *J. Clin. Invest.*, **124**, 111–116.
48. Zhang, A.Y., Mysore, N., Vali, H., Koenekoop, J., Cao, S.N., Li, S., Ren, H., Keser, V., Lopez-Solache, I., Siddiqui, S.N., *et al.* (2016) Choroideremia is a systemic disease with lymphocyte crystals and plasma lipid and RBC membrane abnormalities. *Invest. Ophthalmol. Vis. Sci.*, **56**, 8158–8165.
49. Braverman, N.E. and Moser, A.B. (2012) Functions of plasmalogen lipids in health and disease. *Biochim. Biophys. Acta*, **1822**, 1442–1452.
50. Mohanty, B.P., Bhattacharjee, S., Paria, P., Mahanty, A. and Sharma, A.P. (2012) Lipid biomarkers of lens aging. *Appl. Biochem. Biotechnol.*, **169**, 192–200.
51. Westerfield, M. (2000) *The Zebrafish Book: A Guide for the Laboratory Use of Zebrafish (Danio rerio)*. University of Oregon Press, Eugene.
52. Kimmel, C.B., Ballard, W.W., Kimmel, S.R., Ullmann, B. and Schilling, T.F. (1995) Stages of embryonic development of the zebrafish. *Dev. Dyn.*, **203**, 253–310.
53. Sullivan-Brown, J., Bisher, M.E. and Burdine, R.D. (2011) Embedding, serial sectioning and staining of zebrafish embryos using JB-4 resin. *Nat. Protoc.*, **6**, 46–55.
54. Morash, M.G., Douglas, S.E., Robotham, A., Ridley, C.M., Gallant, J.W. and Soanes, K.H. (2011) The zebrafish embryo as a tool for screening and characterizing pleurocidin host-defense peptides as anti-cancer agents. *Dis. Model Mech.*, **4**, 622–633.
55. Buck, L.M., Winter, M.J., Redfern, W.S. and Whitfield, T.T. (2011) Ototoxin-induced cellular damage in neuromasts disrupts lateral line function in larval zebrafish. *Hear Res.*, **284**, 67–81.
56. Christou-Savina, S., Beales, P.L. and Osborn, D.P. (2015) Evaluation of zebrafish kidney function using a fluorescent clearance assay. *J. Vis. Exp.*, e52540.
57. Wu, Y.W., Alexandrov, K. and Brunsveld, L. (2007) Synthesis of a fluorescent analogue of geranylgeranyl pyrophosphate and its use in a high-throughput fluorometric assay for Rab geranylgeranyltransferase. *Nat. Protoc.*, **2**, 2704–2711.
58. Nguyen, U.T.T., Wu, Y., Goodall, A. and Alexandrov, K. (2010) Analysis of protein prenylation in vitro and in vivo using functionalized phosphoisoprenoids. *Curr. Protoc. Protein Sci.*, **62**, 14.13.11–14.13.15.